Acta of Bioengineering and Biomechanics
Vol. 24, No. 3, 2022

Original paper
DOI: 10.37190/ABB-02134-2022-02

Experimental and numerical analysis of blood flow in roughness impact-*R* test

MAGDALENA KOPERNIK[1]*, DAWID KRUCZEK, PRZEMYSŁAW KURTYKA[2], MAŁGORZATA POMORSKA[2], ROMAN MAJOR[2]

[1] AGH University Science and Technology, Kraków, Poland.
[2] Polish Academy of Sciences, Institute of Metallurgy and Materials Science, Kraków, Poland.

Purpose: The present paper covers simulation of blood flow in a roughness impact-*R* test model to anticipate the hemodynamic conditions of adhesion of blood elements to the modified surface. It was performed using numerical modelling of this process. The aim of these simulations was to create a surface morphology that stimulates the adhesion of blood elements to the surface of base plate of impact-*R* test. *Methods*: The morphology of base plate of impact-*R* test was developed using a vacuum powder sintering of commercial purity titanium powder (CP-Ti) on Ti6Al7Nb substrate. The finite volume method (FVM) and disperse particle method (DPM) were applied to develop the target model of a roughness impact-*R* test. The morphology of modified surfaces was documented with digital microscope and SEM (scanning electron microscopy). *Results*: The impact-*R* test developed using the two-phase blood model performed on regularly structured base plate resulted in shear stress values higher than the analogous for the model lacking such modification. The most significant reduction in maximum values of shear stress occurred in case of the DPM model and especially in the model with regular structures. *Conclusions*: The proposed models are very effective in modeling of the analysis of blood flow in roughness impact-*R* test.

Key words: *finite volume method (FVM), disperse particle method (DPM), two-phase blood model, red blood cells (RBCs), impact-R, roughness*

1. Introduction

The impact-*R* test was developed to study the effect of shear stresses on cardiovascular tissue [40]. Initially, it was designed for laminar flows as a system of two parallel plates to obtain a uniform shear stress distribution, then, modifications were made to obtain oscillating shear stresses, etc. The cone-plate is another system of this test designed to obtain uniform distributions of shear stresses, initially used to measure viscosity of the liquid. Currently, pulse and oscillating shear stresses are generated in this system due to high shear rates. In the case of modern biomedical applications, the system of interest generally corresponds to a laminar three-dimensional flow, and the rotation applied to the cone is usually unstable and periodic. Due to big value of shear rates of rotating cone, the turbulences can be anticipated in the fluid domain of the model. According to literature [8], the analytical solutions can be found using the Π theorem. Six parameters used to characterize the flow (density, dynamic viscosity, axial coordinate, radius, gap height, and angular velocity of the cone) are reduced to formula of the Reynolds number (*Re*). It was experimentally determined [40] that for $Re < 1$ the flow is laminar, axisymmetric and tangential. For $1 \leq Re \leq 4$, the secondary flow effects appear and the laminar flow becomes three-dimensional. For $Re > 4$, the flow is turbulent. The influence of primary and secondary flows on the distribution of shear stress on the surface of the plate was also correlated. These effects were de-

* Corresponding author: Magdalena Kopernik, AGH University of Science and Technology, al. Mickiewicza 30, 30-364 Kraków, Poland. E-mail: kopernik@agh.edu.pl
Received: September 20th, 2022
Accepted for publication: November 4th, 2022

scribed for the unstable rotation of the cone, which has been shown to affect the uniformity of the shear stress distribution on the surface of the plate. The main flow generates the primary stress oriented in the tangential direction, while the secondary flow induced by the centrifugal force produces a secondary stress oriented in the radial direction.

Research on the cone and plate test has focused on the development of the optimal structure [47], experimental tests on blood [36] and on numerical models supporting the analysis of the structure of this test and the obtained results [48]. The work [47] presented analytical solutions for the cone and plate test, which make it possible to calculate the shear stress, and also to indicate the relationship between pressure and angular velocity as well as pressure and the contact surface of the flowing medium. The obtained results showed that the higher the angular velocity of the rotating cone, and the larger the contact area, the lower the pressure. All the above indicate good ultrafiltration properties of such test. Additionally, the shear stress at the edge of the system is homogeneous and, in this test, the mass transfer coefficient depends mostly on the hydrodynamic shear at the contact surface. In paper [36], the effect of deposition of platelets on the surface of polystyrene and the extracellular matrix at set shear rates were investigated. As an outcome, a correlation was observed between the adhesion rate (surface coverage) and the aggregate formation (average size) of platelets from normal citrated blood between polystyrene and extracellular matrix. There was a significant correlation between the results of platelet adhesion (surface coverage) to polystyrene and extracellular matrix ($r^2 = 0.57$). A similar correlation was observed between platelet aggregation rates (average size, $r^2 = 0.63$). In the other study [48], the authors presented a numerical model of the cone and plate test, which was verified experimentally (PIV, particle image velocimetry [43]). It took into account shear stresses at the distance from the center of the system for different both cone angles and in various cone planes. The greater the distance from the center of the system and the smaller the cone angle, the higher the shear stress. Finally, in the work [46], the intensity of turbulence was also analyzed in relation to the distance from the center of the system.

Textured biomaterial surfaces in implantable left ventricular assist devices induce development of a non-thrombotic neointimal surface and allow for elimination of anticoagulation therapy in recipients of such parts [9], [28], [32], [42], [50]. Characterization of the hematopoietic cells formed within the neointimal surfaces of these devices may contribute to our understanding of this problem. Implanting of parts with textured surfaces and subjected to contact with blood leads to a rapid clotting process on the surface. While this may seem like a negative occurrence for blood contact surfaces, it may not be relevant from the clinical point of view. It is because, while clots form quickly on these surfaces, they are densely adherent and do not appear to embolise into the bloodstream, i.e., remain harmless. Over time, additional blood cell interaction occurs, being similar to an immune response. Eventually, a heterogeneous layer containing platelets, monocytes, macrophages, giant cells, lymphocytes and pluripotent hematopoietic cells is deposited on the surface. It is postulated that pluripotent hematopoietic cells differentiate into fibroblasts, myofibroblasts and, in some cases, endothelial cells. Fibroblast cells can then secrete extracellular matrix components such as collagen, which is routinely detected on textured surfaces after prolonged implantation.

The implication of having textured surfaces contacting the blood is that these surfaces rapidly clot upon device placement. A heterogeneous surface containing platelets, monocytes, macrophages, foreign-body giant cells, lymphocytes and multipotent circulating cells is deposited [15], [32], [38]. On a macro scale, such coating may appear to be a solid formation, but according to the literature, the pseudointima undergoes continuous remodeling so as to effectively inhibit the coagulation process at all times. This is a physiologically regulated mechanism under normal conditions and, in this work, in the case of the development of materials with a developed surface, it is nothing more than an attempt to induce a mechanism occurring naturally.

Analyzing the above, one may point out that there is still a need to perform experimental and numerical tests simulating the phenomena on the blood-material contact in blood flow systems. Up till now, experimental and numerical work on the modeling of the blood, flow and ensuring good compliance with the experiment has used, inter alia, mixture theory [24], [25], discrete particle method [49] and SST k-ω turbulence model [21], [45]. Blood flow may also concern issues related to blood-contacting devices, which cause hemolysis [49]. Simultaneously, particle-based models are applied to simulate red blood cells (RBCs) membrane dynamics and platelets as well as margination effects and heterogeneities of blood morphotic elements [5].

The posed problem is the selection of parameters for the surface of the modified materials in contact with blood. However, in the field of modeling blood flows and phenomena on the blood-material contact, there are limitations related to the computational complexity of the proposed models and limitations related

to the biophysics of phenomena that these models should reflect. The successive development of simple and complex models makes it possible to minimize the undesirable effects, i.e., allows for precise determination of the influence of the model parameters on the result and thus enables the development of a model resistant to disturbances. The second problem can be solved by developing a model that introduces the shapes of blood cells, interactions between them and between them and the environment, and the morphology of the surface in contact with blood.

Theoretical considerations concerning this problem [5], [27] cover a discrete phase model of backfilling a morphologically complex surface by RBCs developed to investigate behaviour of the RBCs from a Lagrangian view and a discrete perspective. On the other hand, the goal of the present study is the simulation of blood flow in a roughness impact-*R* test model to anticipate the hemodynamic conditions of adhesion of blood elements to the surface applying FVM (finite volume method) and disperse particle method (DPM). The objective of the experimental studies that inspired the development of the simulation is to create a surface morphology that stimulates the phenomenon of adhesion of blood elements to the modified surface of base plate of impact-*R* test.

2. Materials and methods

2.1. Experimental background

2.1.1. Physical model of impact-*R* test

Testing of materials in the shear stress conditions was performed in the present work with cone and plate analyzer (CPA, Impact-*R*, DiaMed AG, Switzerland), equipped with an optical microscope module, adopted to automatically count number of adherent platelets and their coverage area on the polystyrene (PS) plate (DiaMed Impact-*R* Test Kit) [34], [35]. Polystyrene was a reference material and tested samples were modified by VPS (vacuum powder sintering) on the Ti_6Al_7Nb substrate. The assessment of the biocompatibility of materials was performed through measurements of the platelet count, platelet activation, formation of platelet aggregates, formation of granulocyte-platelet aggregates, and thrombotic potential of generated plasma microparticles. As recommended by the manufacturer, 130 μL of blood was used for each shear stress test and the aliquot of the blood was gently mixed for 60 seconds on the rotational wheel (10 revolutions per minute) to prevent sedimentation of blood cells before each of the replicates. PS surface was the original disposable insert well of the impact-*R* kit, used for testing of platelets. The shear test was used at shear rate 1800 s^{-1} (720 revolutions per minute) for 300 seconds, applying a disposable teflon conical rotor. Following the shear test, the rotor was carefully removed and blood was immediately sampled from the well to the test tubes, for flow cytometry staining. From the remaining blood (80 μL) plasma was separated by centrifugation at 2 000 g for 5 min and stored frozen in −70 °C for further analysis of thrombotic activity.

On the basis of the experimental impact-*R* test, a modified layout shape was built for numerical model of impact-*R*. The modification concerned the base plate (Fig. 1a), which was subjected to corrugation. In order to simulate the topographic conditions after modification with the use of vacuum sintering technology, the following changes and simplifications of the geometry were made. The unevenness of the surface in the model was introduced by cutting 180 μm cubes in the lower layer 500 μm away from each other, what was based on experimental analysis presented in section 2.1.2. and 3. Introducing surface modifications to the model has the same purpose as in the experiment, i.e., to determine whether there is a correlation between surface topography and blood cells adhesion.

According to [40], the wall shear stress τ in cone and plate test can be calculated applying the analytical equation as follows:

$$\tau = \frac{\omega \mu r}{h_0 + r\alpha}, \tag{1}$$

where: ω is the cone angular velocity, α is the cone angle, μ is the dynamic viscosity, r is the plate radius, h_0 is the gap dimension between cone and plate.

Considering presented equation all parameters are known and can be substituted, but the blood dynamic viscosity should be adapted to shear rate $\dot{\gamma}$ obtained in this test [29] and it can be calculated following the formula:

$$\dot{\gamma} = \frac{\omega}{tan\alpha}, \tag{2}$$

where ω is the angular velocity and α is the cone angle.

The small cone angle ensures that the shear rate is constant throughout the shearing gap, this being of particular advantage when investigating time dependent systems because all elements of the sample experience

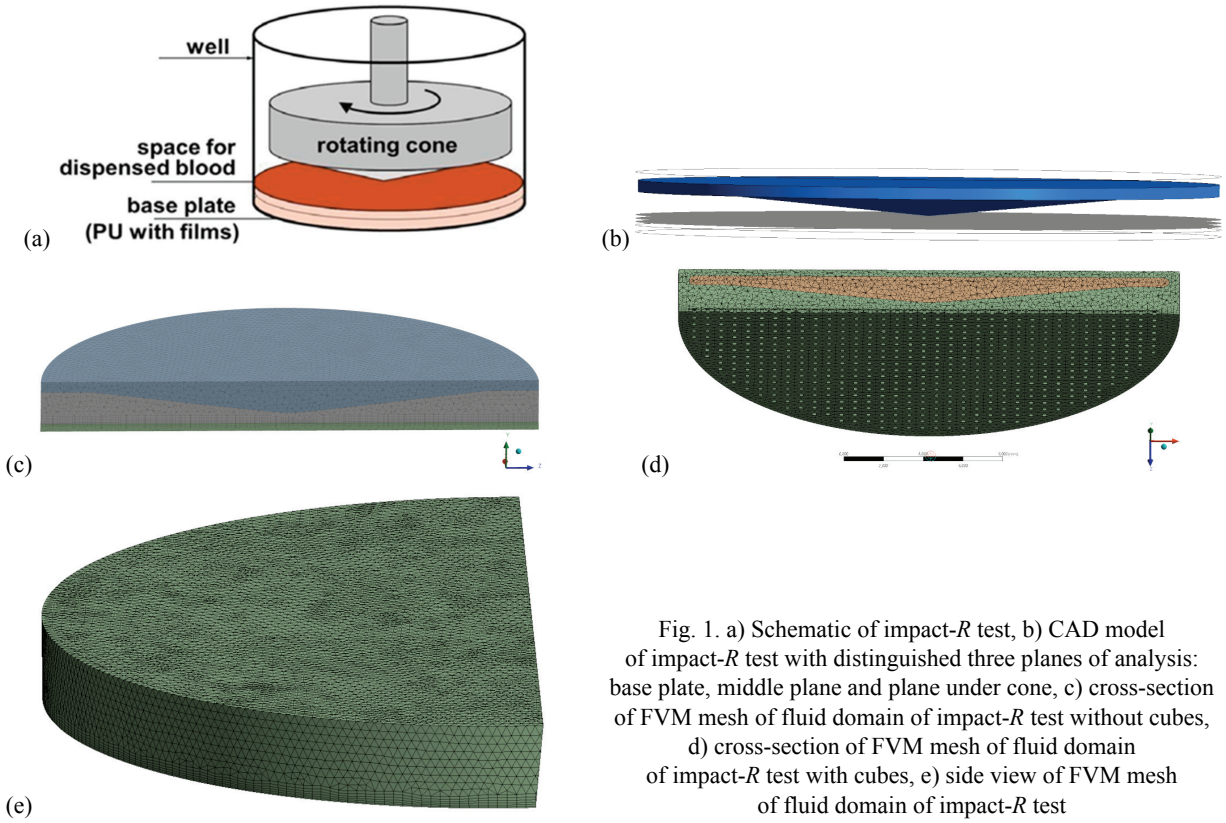

Fig. 1. a) Schematic of impact-*R* test, b) CAD model of impact-*R* test with distinguished three planes of analysis: base plate, middle plane and plane under cone, c) cross-section of FVM mesh of fluid domain of impact-*R* test without cubes, d) cross-section of FVM mesh of fluid domain of impact-*R* test with cubes, e) side view of FVM mesh of fluid domain of impact-*R* test

the same shear history, but the small angle can lead to serious errors arising from eccentricities and misalignment.

According to Eq. (2), the shear rate is much above 1000 s^{-1}. The higher the blood shear rate, the smaller the blood viscosity [11], thus, in the cone and plate test developed in the present paper for example, we can assume μ = 0.003 Pa·s. Substituting values into the analytical simplified Eq. (1) leads to wall shear stress equal to 6.06 Pa. This value strongly depends on dynamic viscosity. For example, if we set dynamic viscosity of μ = 0.001 Pa·s, we get 2 Pa of wall shear stress. The wall shear stress values closer to the analytical solution are computed in models 1 and 2, assuming dynamic viscosity of 0.003 Pa·s. Contrary, the wall shear stress values closer to the analytical solution are computed in models 3 and 4, assuming dynamic viscosity of 0.001 Pa·s. In the paper [8], the calculated value of analytical solution for wall shear stress is lower than computed numerical wall shear stress. The applied dynamic viscosity in [8] was different from the one used in the present paper and it was assumed as for the Newtonian medium. The more comprehensive work [48] shows in details the influence of cone angle, viscosity, angular velocity and gap distance on shear stress computed in the cone and plate test. However, the tested values of parameters are not in the range of values applied in the present paper. Considering work [48], the angular velocity is two times smaller, the gap distance is two time bigger, the dynamic viscosity is three times smaller and the cone angle is also much bigger.

2.1.2. Morphology of the base plate of impact-*R* test

A diversity of surface topography of the Ti_6Al_7Nb substrate was obtained by the vacuum sintering of commercially pure titanium powder CP-Ti (Commercially Pure Titanium). The sintering process was carried out in the Biovac España S.A company, specializing in advanced surface treatment of medical devices and coating of surgical implants. The process parameters were selected accordingly to the holden patent. Titanium powders with two types of grains were used, i.e., in the form of regular spheres (S) and irregular particles (I) in three gradations.

The first attempts to apply VPS technology were promising, including the regularity of the surface and the obtained spaces between surface-fused particles. According to the information available in the literature, an optimal porosity of bioceramics allowing the ingrowth of mineralised and vascularised tissue is in the range of 50–250 μm [3], [4], [41]. Fibroblasts tend to colonise smoother surfaces [10], [17]. In this study, powders in the range of 90–250 μm were used. The

settings of the proposed surface modification covered obtaining a coating of more than 200 μm thickness with a high roughness coefficient and complex morphology. The tests were performed with flat cylindrical samples initially with a diameter of $D = \varnothing 14 \pm 0.02$ mm and a height of $h = 3 \pm 0.02$ mm. In the first step of materials testing, specimens covered with two particle types and three sizes were characterized using scanning electron microscopy (SEM/Quanta 250 FEG, FEI Co., Hillsboro, USA) and digital microscope ZEISS Smartzoom 5 (Carl Zeiss Microscopy, Jena, Germany). Next, an evaluation of the mechanism of cell attachment was documented using SEM microscope.

The contact angle of the samples was tested by optical goniometry on the Möller-Wedel Optical instrument (Möller-Wedel Optical GmbH, Wedel, Germany) at room temperature (approx. 20 °C). Distilled water with a measuring droplet volume of 1.5 μl was used to moisten the surface. Before each measurement, the samples were cleaned and dried from residual water by compressed air.

The surface roughness of the samples was measured using both contact profilometry and optical profilometry in accordance with applicable standards – ISO 21920-2:2021. In the case of contact profilometry, a MAHR XR1 (Mahr GmbH, Göttingen, Germany) semi-automatic device was used, equipped with a BFW A 10-45-2/90° measuring arm. The surface topography was assessed based on the *Ra* and *Rz* parameters, following the statistical principles. In the case of optical profilometry, the Keyence VR-5000 (Keyence Co., Osaka, Japan) 3D optical profilograph was used and the attention was focused mainly on the *Sa* parameter and the qualitative topographic assessment. The *Sa* parameter is an extension of the *Ra* profile parameter in the context of surfaces. This parameter determines the absolute value of points in space as the difference in height with respect to the arithmetic mean value.

2.2. Numerical models

The models included in this paper meet the criteria for numerical models given in [14]. Performed simulations were run using Ansys Fluent 2022 R2 software.

2.2.1. FVM and DPM models of impact-*R* test

In the Ansys Fluent, three different Euler–Euler multiphase models are available. In the present paper, the mixture model has been selected to simulate the two phases of blood: plasma and red blood cells. As in the Eulerian approach, the phases are treated as interpenetrating continua. The mixture model [7] can simulate phases by solving the momentum, continuity and energy equations for the mixture, the volume fraction equations for the secondary phases, and algebraic expressions for the relative velocities. The momentum equation for the mixture can be obtained by summing the individual momentum equations for all phases. It can be expressed as a:

$$\frac{\partial}{\partial t}(\rho_m \vec{v}_m) + \nabla \cdot (\rho_m \vec{v}_m \vec{v}_m) = -\nabla_p + \nabla \cdot [\mu_m (\nabla \vec{v}_m + \nabla \vec{v}_m^T)] + \rho_m \vec{g} + \vec{F} + \nabla \cdot (\Sigma_{k=1}^{n} \alpha_k \rho_k \vec{v}_{dr,k} \vec{v}_{dr,k}), \quad (3)$$

where n is the number of phases, $\vec{F}$ is the body force, and μ_m is the viscosity of the mixture:

$$\mu_m = \Sigma_{k=1}^{n} \alpha_k \mu_k , \quad (4)$$

$\vec{v}_{dr,k}$ is the drift velocity for secondary phase k

$$\vec{v}_{dr,k} = \vec{v}_k - \vec{v}_m . \quad (5)$$

Mixture model simulations were performed for the impact-*R* test with and without cubes on the base plate. Parameters applied in computations for a two phase blood model are presented in Table 1. Mixture model uses Schiller–Naumann drag coefficient.

Table 1. Parameters applied in a two-phase blood model

Parameters	Red blood cells	Blood plasma
Density [kg/m^3]	1 090 [33]	1 040 [33]
Specific heat [J/g°C]	0.87 [31]	3.93 [6]
Thermal conductivity [W/mK]	2.36 [33]	9.93 [33]
Viscosity [kg/ms]	0.0075 [33]	0.0015 [30]
Molecular weight [kg/kmol]	0.0004 [20]	0.018 [1]

The k–ω SST turbulent model is focused on the precision of the k–ω model in the areas close to the wall. The k–ω SST model's transport equations which are used in the Ansys Fluent code are [23]:

$$\frac{\partial(\rho k)}{\partial t} + \frac{\partial}{\partial x_i}(\rho k u_i) = \frac{\partial}{\partial x_j}\left[L_k \frac{\partial k}{\partial x_j} \right] + A_k - B_k , \quad (6)$$

$$\frac{\partial(\rho \omega)}{\partial t} + \frac{\partial}{\partial x_i}(\rho \omega u_i) = \frac{\partial}{\partial x_j}\left[L_\omega \frac{\partial \omega}{\partial x_j} \right] + A_\omega - B_\omega + C_\omega , \quad (7)$$

where: u_i – mean velocity, A_k – production terms of k, B_k – production terms of k, A_ω – production terms of ω, B_k – dissipation terms of k, B_ω – dissipation terms of ω, L_k – effective diffusivity of k, L_ω – effective diffusivity of ω, and C_ω – diffusion term.

In the CFD computations, the applied general power law has the form of:

$$\eta = k\dot{\gamma}^{n-1}, \tag{8}$$

where: η is dynamic viscosity, k is the flow consistence index – 0.013 Pa, $\dot{\gamma}$ is the shear rate and n is the power law index – dimensionless flow behaviour coefficient – 0.7 [37]. The higher the consistency, the higher the viscosity of the fluid. The closer to 1 the power law index is, the more non-Newtonian are the properties of blood.

Discrete phase model [19] was applied in the Ansys Fluent and under assumption that RBCs can interact with blood plasma. The force balance equates the particle inertia with the forces acting on the particle, and can be written (for the x direction in Cartesian coordinates) as [19]:

$$\frac{\partial u_p}{\partial t} = \boldsymbol{F_D}(\boldsymbol{u} - \boldsymbol{u_p}) + \frac{g_x(\rho_p - \rho)}{\rho_p} + \boldsymbol{F_x}, \tag{9}$$

where: $\boldsymbol{u}$ is the fluid phase velocity, $\boldsymbol{u_p}$ is the particle velocity, $\boldsymbol{F_x}$ is the additional acceleration (force/unit particle mass) term, ρ is the fluid density, ρ_p is the density of the particle, $\boldsymbol{F_D}(u - u_p)$ is the drag force per unit particle mass and:

$$\boldsymbol{F_D} = \frac{18\mu}{\rho_p d_p^2} + \frac{C_D Re}{24}, \tag{10}$$

where: μ is the molecular viscosity of the fluid, d_p is the particle diameter and C_D is the drag coefficient, Re is the Reynolds number.

Thus, in the Ansys Fluent software, the particles are modelled as spheres with ascribed density and a particle size distribution based on the experimental distributions. The discrete phase is modelled using the Lagrangian approach with Fluent's DPM. The Lagrangian tracking method is used to solve the individual trajectories of the theoretical particles by equating their inertia with external forces.

Two-way coupling, i.e., the exchange of momentum between the particles and fluid, is accounted for. The framework of the model also involves particle-wall collisions, particle–particle collisions and structure dependent drag. The spherical drag proposed by Morsi and Alexander is used to model the particle behaviour. Particle–particle collisions are accounted for by using the Nanbu–Babovsky collision model. This is a stochastic collision approach where the probability of a collision between proach where the probability of a collision between particles is based on the volume of particles within a cell and their relative velocities.

2.2.2. FVM and DPM model assumptions

FVM (finite volume method) models were developed in the Ansys Fluent 2022 R2 software to compare the effect of applying different blood models and roughness of base plate of impact-*R* test with the aim to investigate their influence on blood velocity and shear stress.

The developed simulations were run on a standard PC (Processor Intel® Core ™ i7-3770 CPU, 3.40 GHz, 24 GB RAM). The simulations lasted for 0.083 s (1000 iterations) with time step of $8.3 \cdot 10^{-5}$ s. The FVM (finite volume method) mesh of impact-*R* test without cubes was composed of 497 557 cells and 147 379 nodes. The mesh quality parameters (skewness – 0.09, orthogonal quality – 0.9, element quality – 0.8) were very good and there were 6 layers of prism elements near walls of the FVM model. The average element size was 0.276 mm. The FVM mesh of impact-*R* test with cubes was composed of 477 553 cells and 122 159 nodes. The average element size was 0.26 mm. The mesh quality parameters (skewness – 0.08, orthogonal quality – 0.8, element quality 0.7) were very good and there were 6 layers of prism elements near walls of the FVM model. The views of developed FVM meshes of impact-*R* test models without and with cubes are shown in Fig. 1. The developed FVM model of impact-*R* test uses non-Newtonian power law [26] and the following coefficients of blood are assumed to be: density 1059 kg/m^3 [13], specific heat 3617 J/kgK [22] and thermal conductivity 0.52 W/mK [46].

The pressure-based solver and absolute velocity formulation were selected for computational purpose. The pressure-velocity coupling scheme of solution was selected with spatial discretization using gradient (least squares cell-based) and transient formulation was also used. Finally, the SST k–ω turbulence model [20], [47] was applied in all simulations.

The cubes generated on the base plate of impact-*R* test model had dimensions of 180 μm and the distance among them was 500 μm. In the Ansys Fluent, three different Euler–Euler multiphase models were available. In the present study, the mixture model has been selected to model the two phases of blood: plasma and RBCs. Parameters applied in computations for the two phase blood model are presented in Table 1 [1], [6], [20], [30], [31], [33].

DPM models were developed to compare the effect of application of cubes on the base plate of impact-*R*

test model as well as to compute distributions of RBCs mass concentration and velocity magnitude, etc. A DPM model of backfilling a morphologically complex surface by RBCs was developed to investigate the behavior of the RBCs from a Lagrangian view and a discrete perspective. Blood behavior in Lagrangian view was examined on the basis of a particle tracking of a RBC of blood plasma flow whereas blood plasma behavior was considered in Eulerian view based on the assumption of a finite volume element in the fluid flow path. In modeling of RBC – primary blood plasma interaction a two way approach was considered, in which RBC fluid flow and carrier blood plasma flow interact with each other simultaneously.

The diameter of RBCs was assumed to be 5–10 μm using the Rosin–Rammler diameter distribution method. The rotation of RBCs was enabled. The density of plasma was 1040 kg/m^3, specific heat – 3930 J/kgK, thermal conductivity – 9.93 W/mK and viscosity was 0.0015 kg/ms [6], [31]. The density of RBCs equaled to 1090 kg/m^3 and specific heat equaled to 870 J/kgK [31]. Viscosity of red blood cells was set to 0.0075 kg/ms and their surface tension to $5 \cdot 10^{-6}$ N/m [2].

Particles and plasma were injected in full volume and the system had no other physical inlet. In simulation, particles were injected into the entire volume of the medium, just like in the performed experiment. This allowed the behavior of particles to be observed without imposing additional boundary conditions at the inlet, i.e., helped to eliminate it directly. The total flow rate of RBCs was $1 \cdot 10^{-10}$ kg/s. The DPM model is characterized by an interaction with continuous phase and a particle track with fluid flow time step. The boundary condition of RBCs phase is assumed as escape, however RBCs can be reflected from the ground.

3. Results

In the case of digital microscopy, the tests were carried out with the use of 500× and 1000× magnification with the use of the 3D stitching module. As far as scanning microscopy is concerned, the observations were carried out in high vacuum conditions with a maximum value of 3.5×10^{-4} Pa using an ETD detector (Everhart–Thornley Detector) with an accelerating voltage of 5 kV. In the present study, the regular structure of titanium powders has inspired the development of the numerical models with modified surface. The modification of the surface was introduced by cutting 180 μm cubes in the lower layer with a distance of 500 μm between them, what was based on the experimental observation made using digital microscopy (side view, 100× magnification, Fig. 2) and SEM (200, 250, 500 and 600× magnification, Fig. 3). The selected results of SEM analysis shown in Figs. 3c–e represent surface of regular structure of titanium powder after contact with blood what is manifested by RBCs adhered on the spheres, in surface imperfections and between spheres. The attachment of blood morphotic elements was observed mainly in the corners of the structures between the powder grains. Thus, it confirms the validity of developing coatings with a high degree of differentiation or porosity.

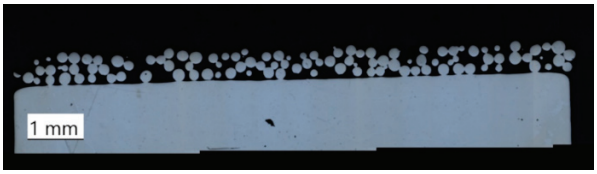

Fig. 2. Microscopic analysis of materials with modified surface using digital microscopy techniques for surface with regular structure for magnification 100×

Changes in the contact angle during 60 sec for each measurement were determined based on the image analysis. All samples after modification with the vacuum powder sintering method for the proposed powders are characterized by a contact angle of $\theta = 103° \pm 4$.

Based on the roughness test an increase in *Ra*/*Rz* and *Sa* parameters was observed with an increase in the grain size of the powders used during the modification. The *Ra* parameter was in the range of 20–48 μm, and the *Sa* surface roughness parameter for the spherical modification was in the range of 28–58 μm, and for the irregular modification – 25–56 μm. Thus, no significant influence of the powder morphology on the degree of surface roughness was observed. With the use of a digital microscope and scanning microscopy, a high degree of differentiation of the topography of the coatings was observed due to the morphology of the powders used, i.e., spherical and irregular powder. The coatings formed as a result of the S modification had a regular structure with rounded shapes. Modification I resulted in the formation of a coating with numerous irregular elevations and craters. Based on the cross-sectional analysis, the thickness of the formed coatings was estimated to be in the range of $h = 265$–526 μm for modification S and $h = 202$–735 μm for modification I. Moreover, with the use of image analysis software, it was possible to assess the degree of porosity of the obtained coatings and the dependence resulting from the influence of the powder sizes. The analysis of the coating porosity and the presence of open and

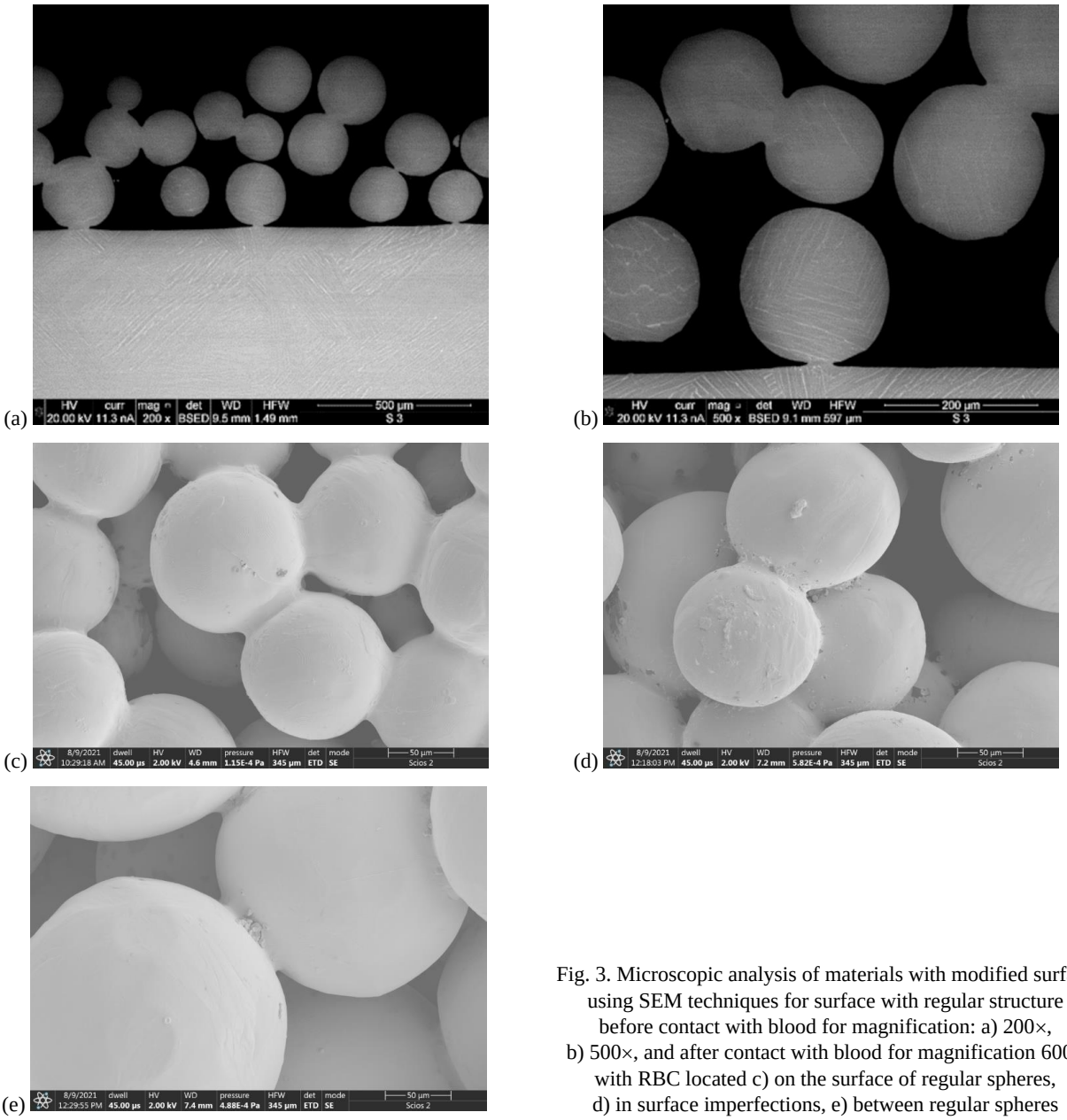

Fig. 3. Microscopic analysis of materials with modified surface using SEM techniques for surface with regular structure before contact with blood for magnification: a) 200×, b) 500×, and after contact with blood for magnification 600× with RBC located c) on the surface of regular spheres, d) in surface imperfections, e) between regular spheres

closed pores as well as their size are key issues related to the potential of cells and tissue anchoring for permanent integration with the implant. The direct increase in porosity is visible along with the grain size of the powders used. In the case of the S modification, the obtained coatings are characterized by a greater porosity than the samples after modification I, in the range of 41–47%. The coatings obtained with the use of irregular powders had a porosity of 29–37%.

The results of computations shown in this section are independent either of time step, number of iterations and density or quality of computational mesh. Introduction of cubes in the DPM model were preceded by analysis of its influence on the CFD simulations. The comparison of CFD and DPM simulations of blood flow for models without and with cubes on the base plate of impact-*R* test are shown in Figs. 4 and 5 for selected cross-sections of the blood flow domain (planes 1–3: base plate, middle plane and plane under cone, Fig. 1b) considering averaged blood velocity (Fig. 4) and shear stress (Fig. 5). In Figure 6, the results of blood velocity and shear stress computed for planes 1–3 of the following versions of model of impact-*R* test named briefly as "models 1–6", are shown as following: model 1 – applying single phase blood model and base plate without cubes, model 2 – applying single phase blood model and base plate with cubes, model 3 – applying two phase blood model and base plate without cubes, model 4 – applying two phase blood model and base plate with cubes, model 5 – applying DPM model without cubes, and model 6 – applying

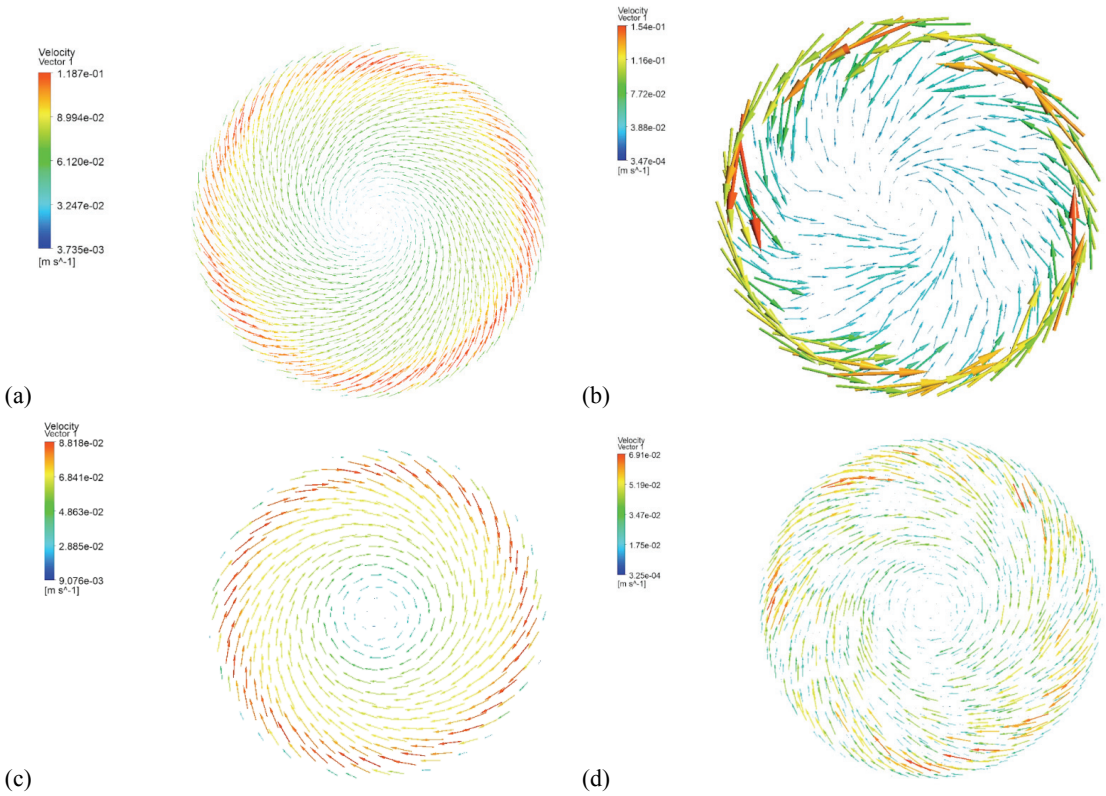

Fig. 4. Distributions of blood velocity of impact-*R* test model computed on plane 1 under cone in: (a) model 3, (b) model 4, (c) model 5, and (d) model 6

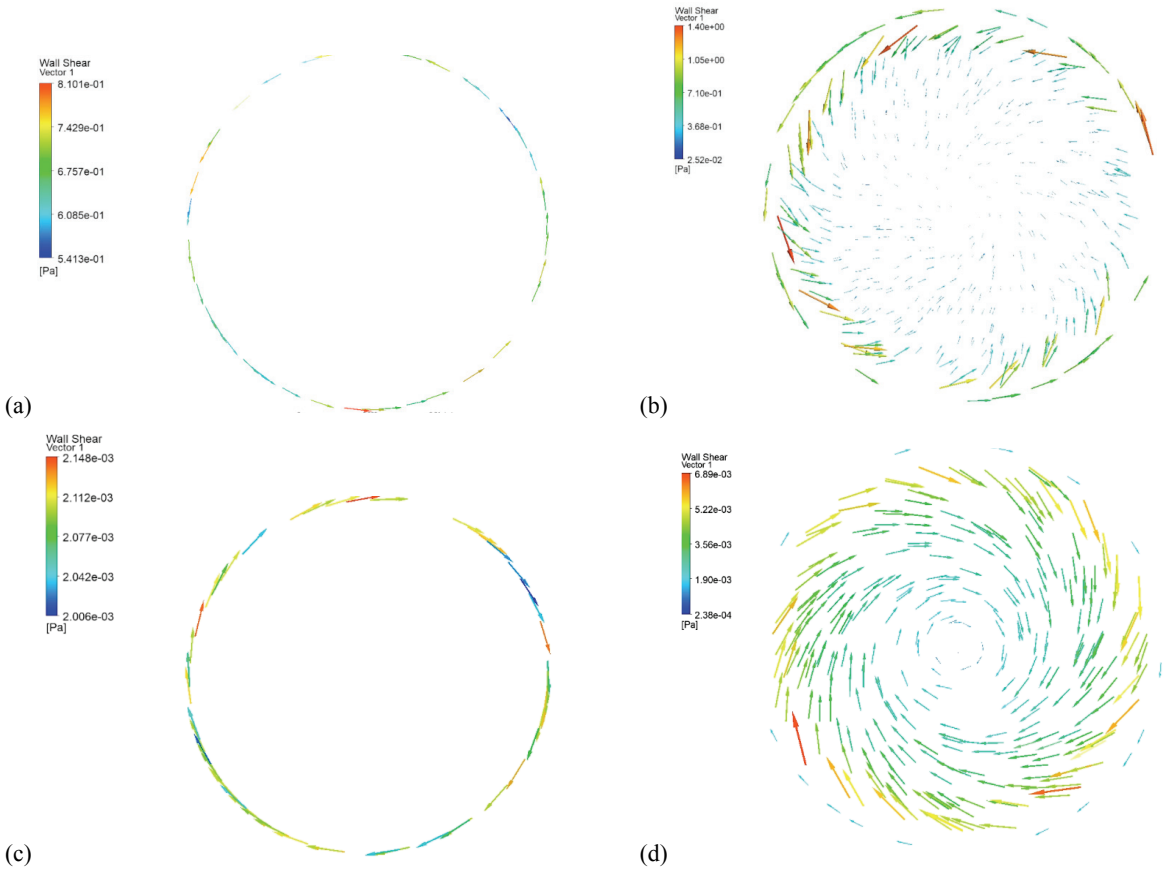

Fig. 5. Distributions of wall shear stress of impact-*R* test model computed on plane 1 cone in: (a) model 3, (b) model 4, (c) model 5, and (d) model 6

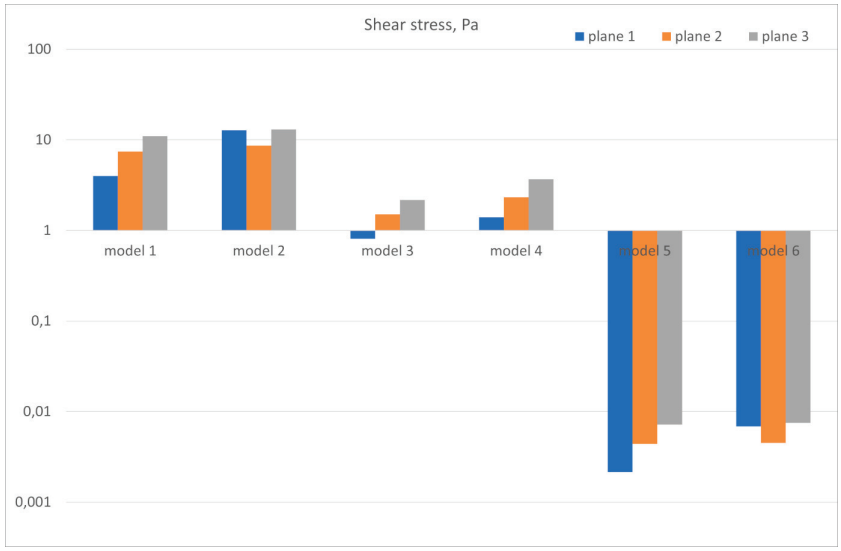

(b)

Fig. 6. Graphs of maximum values of: (a) blood velocity and (b) wall shear stress of impact-*R* test model computed on planes 1–3 under cone in models 1–6

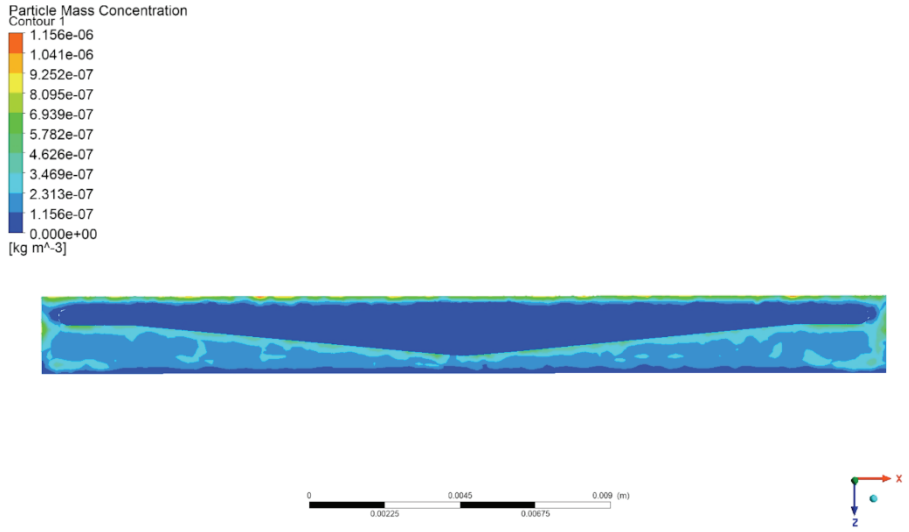

(a)

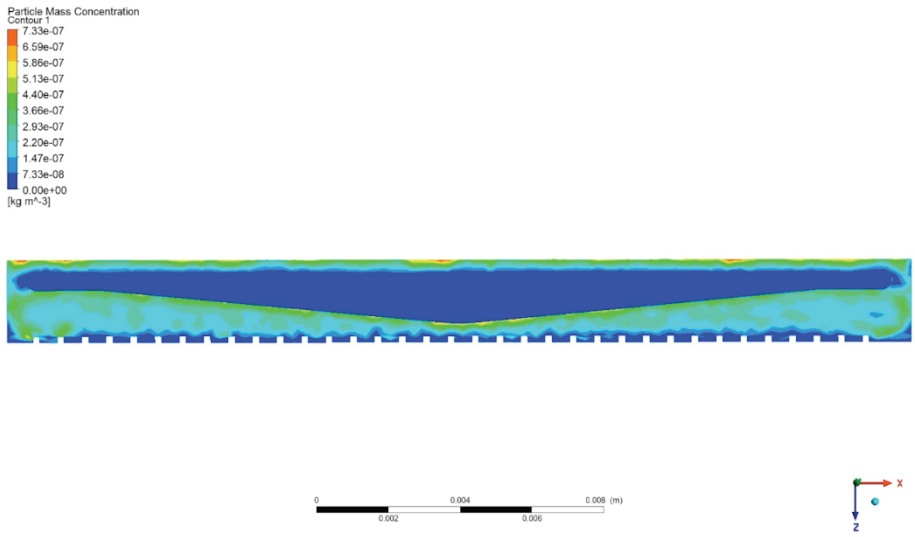

(b)

Fig. 7. Distributions of RBCs mass concentration on the cross-section of: (a) model 5, and (b) model 6

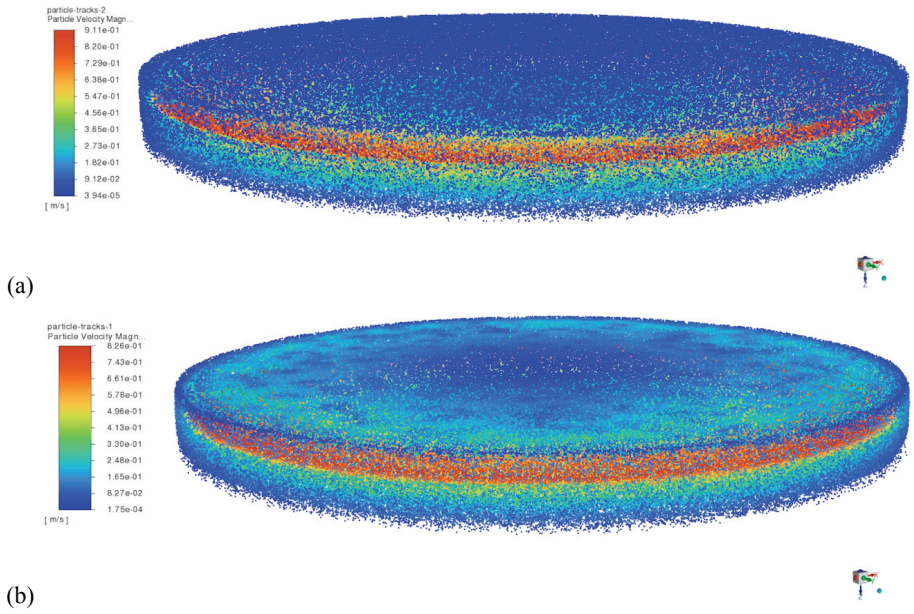

Fig. 8. Distributions of RBCs velocity magnitude in: (a) model 5, and (b) model 6

DPM model with cubes. Global DPM results such as RBCs mass concentration and RBCs velocity magnitude in the models 5 and 6 are shown in Figs. 7 and 8. The results presented in Figs. 7 and 8 are generated according to the procedure – Lagrangian Particle Tracking.

4. Discussion

A qualitative analysis of the results obtained for the selected planes under the cone of impact-*R* test shows that for each of the models the blood velocity decreases from perimeter towards the center of the model where it reaches minimum values (Fig. 4). For example, in model 3, on the base plate, the maximum velocity is 0.1187 m·s^{-1} (Fig. 4a) and in model 4, the maximum velocity is 0.154 m·s^{-1} (Fig. 4b). Model 5 on the base plate results in the maximum velocity of 0.08818 m·s^{-1} (Fig. 4c) and model 6 results in the maximum velocity of 0.0691 m·s^{-1} (Fig. 4d). The most significant reduction in values of blood velocity occurs in the DPM model with cubes, especially on the base plate. The use of multiphase blood models does not affect the character of distributions of blood velocity. The introduction of the cubes on the base plate of impact-*R* test leads to larger velocity gradients around the circumference (Figs. 4b, d). It is because the flowing blood washes the cubes. Applying a model of impact-*R* with a greater density of cubes than presented in this paper (less than distance of 500 µm among cubes), results in blood reflection from the surface of cubes and stop of the blood flow under the cone consistent with its rotation.

Presence of the porous surfaces result in greater adhesion and activation during the blood flow. The rebound effect does not depend on topography, but rather on the chemical and physical properties of the surface. As for the physical properties, it is the contact angle that determines the reflection phenomenon in the first place. All samples after modification with the vacuum sintering method for the proposed powders are characterized by a contact angle of $\theta = 103° \pm 4$, what can be attributed to their hydrophobic character. RBCs adhere in various places on the modified surface, both regular and irregular. After blood incubation, coatings were analyzed by SEM to evaluate the mechanism of cell attachment to the textured surface. As a result, the attachment of blood morphotic elements was observed mainly at the corners of the structures connecting adjacent powder particles (Fig. 3). Therefore, it confirmed the necessity to determine the correlation between topography surface diversity and cells attachment. In the case of the S modification, the obtained coatings are characterized by a greater porosity than the samples after modification I, in the range of 41–47%.

In the case of simulations of impact-*R* test without cubes, the shear stresses occur only on the circumference of the base plate. In model 3, on the base plate, the maximum shear stress is 0.81 Pa (Fig. 5a) and in model 4 the shear stresses reach large gradients on the perimeter where maximum shear stress is 1.4 Pa (Fig. 5b), and much lower values in its center where the maximum shear stress is 0.02 Pa, which is due to

location of the cubes. In model 5, on the base plate, the maximum shear stress is 0.0021 Pa (Fig. 5c) and in model 6, the shear stresses reach large gradients on the perimeter where maximum shear stress is only 0.0069 Pa (Fig. 5d), and much lower values in its center where the maximum shear stress is only 0.0002 Pa. The most significant reduction of shear stress occurs in the DPM model and especially in the model with cubes. In the DPM models, the closer to the surface under the cone, the lower the shear stress. This fact is similar to the observation done in [48].

The quantitative analysis of the results obtained for the 3 planes (compare Section 3) in 6 versions of impact-*R* test models shows that the highest blood velocities (just over 0.3 $m \cdot s^{-1}$, Fig. 6a) are present in model 4 under cone. The simulations of impact-*R* test developed using single phase blood model show the maximum shear stresses (about a dozen Pascals, Fig. 6b), while the simulations with two-phase blood model (model 3 and 4) present shear stresses significantly lower (about a few Pascals, Fig. 6b) and their distributions are uniform starting the analysis from plane 1 to plane 3. In the case of the simulations of impact-*R* test developed using the two-phase blood model and cubes (model 4) on the base plate, the shear stresses are slightly higher (shear stress of 4 Pa under cone) than in the analogous simulations without cubes (model 3, shear stress of 2 Pa under cone). In the case of the simulations of impact-*R* test developed using the DPM model and cubes on the base plate, the shear stresses are very low and the differences in computed results between the model 5 and 6 are less significant, as well as among different planes for a given DPM model. In the developed DPM models, the hematocrit is high, the concentration of blood cells is high, so the viscosity also increases. This also has to do with the reduction of shear stress (increased viscosity).

In the case of no-slip boundary condition applied in the impact-*R* test, we only deal with shear stresses resulting from the interaction of cell adhesion molecules with surface what has been also shown in other experiments [12], [44]. The maximum wall shear stresses obtained in literature for the impact-*R* test are from 0.3 Pa in [8] to 7 Pa in [39] for models without roughness. So, in this work, the computed wall shear stresses from 0.0021 Pa to 13 Pa are almost in the range of literature data, however these models of impact-*R* test comprise roughness. In the present paper, the obtained tangential distributions of wall shear stress and velocity distributions increasing from the center of the model to its edge coincide with experimental and literature observations [8], [39]. The impact-*R* test model developed in the present study comprises roughness of the sample and blood flow turbulence, thus the presented results show output of the blood-material interaction. Introducing roughness in the impact-R test model affects the increase of wall shear stress (Fig. 6b), therefore, such model of impact-*R* test better anticipates distributions of velocities and shear stresses.

A comparative analysis of single-phase blood models, two-phase blood models and RBCs models shows that the influence of particles on the computed parameters is significant and the selection of the model with particles is appropriate in the context of micro-level phenomena, which one or two-phase models are unable to account for.

The global DPM model results (RBCs mass concentration and RBCs velocity magnitude) computed for the model with cubes (model 6) show lower values than the DPM model without cubes (model 5), what is presented in Figs. 7 and 8. The highest velocities and mass concentrations of RBCs are calculated on the upper surface of the rotating cone in the impact-*R* test (Figs. 7 and 8). Both RBCs velocities and RBCs mass concentrations are not maximum under cone. The local increase in RBCs mass concentration (model 6, Fig. 7b) also takes place between the cubes in the middle part of the model, as in the zone close to its inner wall. Such local mass concentrations can result in local deposition of red blood cells, what was observed in the experiment. Local RBCs mass concentrations also occur in the model without cubes (model 5, Fig. 7a), so they are most likely being the direct result of the flow itself.

As it concerns the blood contact devices, it is important to better understand the relationship between shear stress, exposure time and blood damage. An example of blood damage is not only causing the hemolysis or activation of platelets, but also thrombosis and embolism as well as the destruction of von Willebrand factor (vWf). According to the literature, hemolysis occurs at shear stress level (SSL) > 150 Pa, activation of thrombocytes > 50 Pa and degradation of von Willebrand factor > 9 Pa [15]. *In vitro* testing for hemocompatibility remains a challenge because the background of interactions between blood and foreign material is not fully explained [18]. It is generally acknowledged that initial and rapid adsorption of plasma proteins can establish further biocompatible properties of the material [16], [36]. The process can be quite selective, as evidenced for PS surface, which covers with large proteins, including von Willebrand factor, a major docking molecule for platelet. From the practical point of view, quality of the surface of the material is also very important. During blood flow any rough surface, its

protuberances or cavities, can result in non-laminar flow, and precipitate cells activation and adhesion. Physiological endothelium has very smooth surface, because the cells are flattened to much less than 1 μm thickness. The major limitation of *in vitro* tests for hemocompatibility is due to a short time of the experiment.

5. Conclusions

The introduction of cubes on base plate of impact-*R* test model leads to increased velocity gradients around the circumference. The highest values of the blood velocity were obtained in the simulations with two-phase blood model and cubes on the base plate.

The simulations of impact-*R* test developed using single-phase blood models show the highest values of shear stresses. The simulation of impact-*R* test developed using the two-phase blood model and cubes on the base plate results in the shear stresses slightly higher (shear stress of 4 Pa under cone) than the analogous simulation without cubes. The most significant reduction in shear stresses occurs in simulation with the DPM model and especially applying cubes.

The shear stress level obtained from the simulations of impact-*R* test is below critical, which is dangerous for blood morphotic elements. However, application of single phase blood model and cubes in the simulation of impact-*R* test results in shear stress above the safety level given by von Willebrand factor.

The powders' morphology has no significant effect on the degree of surface roughness. However, a strong differentiation of the coating's topography was observed due to the varying morphology of the used powders. One of the outcomes was an increase in porosity noted along with the growing powders' particle size. After modification with the vacuum sintering method for the proposed powders all samples showed hydrophobic character.

Acknowledgements

The work was executed under fundamental research No. 16.16.110.663 financed by AGH University of Science and Technology.

References

[1] ADAMCZUK K., WOLAŃSKI W., KASPERA W., *Analysis of blood flow in the cerebral arteries*, Curr. Probl. Biomech., 2016, 11, 9–14 (in Polish).

[2] ALIMOHAMADI H., SMITH A., NOWAK R., FOWLER V., RANGAMANI P., *Non-uniform distribution of myosin-mediated forces governs red blood cell membrane curvature through tension modulation*, PloS. Comput. Biol., 2020, 16, 1–26.

[3] BARBA A., DIEZ-ESCUDERO A., MAAZOUZ Y., RAPPE K., ESPANOL M., MONTUFAR E.B., BONANY M., SADOWSKA J.M., GUILLEM-MARTI J., ÖHMAN-MÄGI C., PERSSON C., MANZANARES M.C., FRANCH J., GINEBRA M.P., *Osteoinduction by Foamed and 3D-Printed Calcium Phosphate Scaffolds: Effect of Nanostructure and Pore Architecture*, ACS Appl. Mater. Interfaces, 2017, 9, 41722–41736.

[4] BASIAGA M., PASZENDA Z., LISOŃ J., TARATUTA A., KAZEK-KĘSIK A., KROK-BORKOWICZ M., NUCKOWSKI P., SZINDLER M., STASZUK M., MAJOR Ł., MAJOR R., ČECH BARABASZOVÁ K., DYNER M., *Microstructure and antibacterial properties of a ZnO coating on a biomaterial surface*, Arch. Civ. Mech. Eng., 2022, 22, DOI: 10.1007/s43452-022-00414-8.

[5] BERIS A.N., HORNER J.S., JARIWALA S., ARMSTRONG M.J., WAGNER N.J., *Recent advances in blood rheology: A review*, Soft Matter., 2021, 17, 10591–10613.

[6] BLAKE A.S.T., PETLEY G.W., DEAKIN C.D., *Effects of changes in packed cell volume on the specific heat capacity of blood: implications for studies measuring heat exchange in extracorporeal circuits*, Br. J. Anaesth., 2000, 84, 28–32.

[7] BOWEN R.M., *Incompressible porous media models by use of the theory of mixtures*, Int. J. Eng. Sci., 1980, 18, 1129–1148.

[8] BUSCHMANN M.H., DIETERICH P., ADAMS N.A., SCHNITTLER H.-J., *Analysis of flow in a cone-and-plate apparatus with respect to spatial and temporal effects on endothelial cells*, Biotechnol. Bioeng., 2005, 89, 493–502.

[9] CAI Q., LIAO W., XUE F., WANG X., ZHOU W., LI Y., ZENG W., *Selection of different endothelialization modes and different seed cells for tissue-engineered vascular graft*, Bioact. Mater., 2021, 6, 2557–2568.

[10] CANULLO L., GENOVA T., GROSS TRUJILLO E., PRADIES G., PETRILLO S., MUZZI M., CAROSSA S., MUSSANO F., *Fibroblast Interaction with Different Abutment Surfaces: In Vitro Study*, Int. J. Mol. Sci., 2020, 21, DOI: 10.3390/ijms21061919.

[11] CONNES P., ALEXY T., DETTERICH J., ROMANA M., HARDY-DESSOURCES M.-D., BALLAS S.K., *The role of blood rheology in sickle cell disease*, Blood Rev., 2016, 30, 111–118.

[12] DERAKHTI S., HAMID SAFIABADI-TALI S., AMOABEDINY G., SHEIKHPOUR M., *Attachment and detachment strategies in microcarrier-based cell culture technology: A comprehensive review*, Mat. Sci. Eng. C, 2019, 103, DOI: 10.1016/j.msec.2019.109782.

[13] EL-ARAGI G.M., *Effect of electrohydraulic discharge on viscosity of human blood*, Phys. Res. Int., 2013, DOI: 10.1155/2013/203708.

[14] ERDEMIR A., GUESS T.M., HALLORAN J., TADEPALLI S.C., MORRISON T.M., *Considerations for reporting finite element analysis studies in biomechanics*, J. Biomech., 2012, 45, 625–633.

[15] FRASER K.H., ZHANG T., TASKIN M.E., GRIFFITH B.P., WU Z.J., *A quantitative comparison of mechanical blood damage parameters in rotary ventricular assist devices: shear stress, exposure time and hemolysis index,* J. Biomech. Eng., 2012, 134, DOI: 10.1115/1.4007092.

[16] GEMMEL C.H., *Activation of platelets by* in vitro *whole blood contact with materials: increases in microparticle procoagu-*

lant activity, and soluble P-selectin blood levels, J. Biomater. Sci. Polym. Ed., 2001, 12, 933–943.

[17] GHEISARIFAR M., THOMPSON G.A., DRAGO C., TABATABAEI F., RASOULIANBOROUJENI M., In vitro *study of surface alterations to polyetheretherketone and titanium and their effect upon human gingival fibroblasts*, J. Prosthet. Dent., 2021, 125, 155–164.

[18] HARRISON P., *Progress in the assessment of platelet function*, Br. J. Hematol., 2000, 111,733–744.

[19] HEINRICH M., SCHWARZE R., *3D-coupling of Volume-of-Fluid and Lagrangian particle tracking for spray atomization simulation in OpenFOAM*, Software X, 2020, 11, DOI: 10.1016/j.softx.2020.100483.

[20] HIMBERT S., ALSOP R., ROSE M., *The Molecular Structure of Human Red Blood Cell Membranes from Highly Oriented, Solid Supported Multi-Lamellar Membranes*, Sci. Rep., 2017, 7, DOI: 10.1038/srep39661.

[21] JAMES M.E., PAPAVASSILIOU D.V., O'REAR E.A., *Use of computational fluid dynamics to analyze blood flow, hemolysis and sublethal damage to red blood cells in a bileaflet artificial heart valve*, Fluids, 2019, 4, DOI: 10.3390/fluids4010019.

[22] KARAKI W., RAHUL F.N.U., LOPEZ C.A., BORCA-TASCIUC D.A., DE S., *A continuum thermomechanical model of in vivo electrosurgical heating of hydrated soft biological tissues*, Int. J. Heat Mass Transf., 2018, 127, 961–974.

[23] KHANJANPOUR M.H., JAVADI A.A., *Experimental and CFD analysis of impact of surface roughness on hydrodynamic performance of a darrieus hydro (DH) turbine*, Energies, 2020, 13, DOI: 10.3390/en13040928.

[24] KIM J., ANTAKI J.F., MASSOUDI M., *Computational study of blood flow in microchannels*, J. Comput. Appl. Math., 2016, 292, 174–187.

[25] KOPERNIK M., TOKARCZYK P., *Development of multi-phase models of blood flow for medium-sized vessels with stenosis*, Acta Bioeng. Biomech., 2019, 21, 63–70.

[26] KOPERNIK M., DYRDA K., KURTYKA P., MAJOR R., *Discrete phase model of blood flow in a roughness microchannel simulating the formation of pseudointima*, Acta Bioeng. Biomech., 2022, 24, 131–144.

[27] MAHDAVIMANESH M., NOGHREHABADI A.R., BEHBAHANINEJAD M., AHMADI G., DEHGHANIAN M., *Lagrangian Particle Tracking: Model Development*, Life Sci. J., 2013, 10, 34–41.

[28] MENCONI M.J., POCKWINSE S., OWEN T.A., DASSE K.A., STEIN G.S., LIAN J.B., *Properties of blood-contacting surfaces of clinically implanted cardiac assist devices: gene expression, matrix composition, and ultrastructural characterization of cellular linings*, J. Cell. Biochem., 1995, 57, 557–573.

[29] NADER E., SKINNER S., ROMANA M., FORT R., LEMONNE N., GUILLOT N., GAUTHIER A., ANTOINE-JONVILLE S., RENOUX C., HARDY-DESSOURCES M.-D., STAUFFER E., JOLY P., BERTRAND Y., CONNES P., *Blood Rheology: Key Parameters, Impact on Blood Flow, Role in Sickle Cell Disease and Effects of Exercise*, Front. Physiol., 2019, 10, 1329, DOI: 10.3389/fphys.2019.01329.

[30] PEDERSEN L., NIELSEN E.B., CHRISTENSEN M.K., BUCHWALD M., NYBO M., *Measurement of plasma viscosity by free oscillation rheometry: imprecision, sample stability and establishment of a new reference range*, Ann. Clin. Biochem., 2014, 51, 495–498.

[31] PONDER E., *The specific heat and the heat of compression of human red cells, sickled red cells, and paracrystalline rat red cells*, J. Gen. Physiol., 1995, 38, 575–580.

[32] RAFFI S., OZ M.C., SELDOMRIDGE J.A., FERRIS B., ASCH A.S., NACHMEN R.L., SHAPIRO F., ROSE E.A., LEVIN H.R., *Characterisation of hematopoetic cells arising on the textured surface on left ventricular assist devices*, Ann. Thorac. Surg., 1995, 60, 1627–1632.

[33] ROSENTRATER K.A., FLORES R.A., *Physical and rheological properties of slaughterhouse swine blood and blood components*, T. ASAE., 1997, 40, 683–689.

[34] SANAK M., JAKIEŁA B., WĘGRZYN W., *Assessment of hemocompatibility of materials with arterial blood flow by platelet functional tests*, Bull. Pol. Acad. Sci. Tech., 2010, 58, 317–322.

[35] SCHAUB R.D., KAMENEVA M.V., BOROVETZ H.S., WAGNER W.R., *Assessing acute platelet adhesion on opaque metallic and polymeric biomaterials with fiber optic microscopy*, J. Biomed. Mater. Res., 2000, 49, 460–468.

[36] SHENKMAN B., SAVION N., DARDIK R., TAMARIN I., VARON D., *Testing of Platelet Deposition on Polystyrene Surface Under Flow Conditions by the Cone and Plate(let) Analyzer: Role of Platelet Activation, Fibrinogen and von Willebrand Factor*, Thromb. Res., 2000, 99, 353–361.

[37] SHEWAFERAW S.S., COLLINS W.E., *The Rheology of Blood Flow in a Branched Arterial System*, Appl. Rheol., 2005, 15, 398–405.

[38] SPANIER T., OZ M., LEVIN H., WEINBERG A., STAMATIS K., STERN D., ROSE E., SCHMIDT A.M., *Activation of coagulation and fibrinolytic pathways in patients with left ventricular assist devices*, J. Thorac. Cardiovasc. Surg., 1996, 112, 1090–1097.

[30] SPRUELL C., BAKER A.B., *Analysis of a high-throughput cone-and-plate apparatus for the application of defined spatiotemporal flow to cultured cells*, Biotechnol. Bioeng., 2013, 110, 1782–1793.

[40] SUCOSKY P., PADALA M., ELHAMMALI A., BALACHANDRAN K., JO H., YOGANATHAN A.P., *Design of an* ex vivo *culture system to investigate the effects of shear stress on cardiovascular tissue*, J. Biomech. Eng., 2008, 130, DOI: 10.1115/1.2907753.

[41] TANIGUCHI N., FUJIBAYASHI S., TAKEMOTO M., SASAKI K., OTSUKI B., NAKAMURA T., MATSUSHITA T., KOKUBO T., MATSUDA S., *Effect of pore size on bone ingrowth into porous titanium implants fabricated by additive manufacturing: An in vivo experiment*, Mater. Sci. Eng. C Mater. Biol. Appl., 2016, 59, 690–701.

[42] THYAGARAJAN B., KUMAR M.P., SIKACHI R.R., AGRAWAL A., *Endocarditis in left ventricular assist device*, Intractable Rare Dis. Res., 2016, 5, 177–184.

[43] TOMASZEWSKI M., SYBILSKI K., MAŁACHOWSKI J., WOLAŃSKI W., BUSZMAN P.P., *Numerical and experimental analysis of balloon angioplasty impact on flow hemodynamics improvement*, Acta Bioeng. Biomech., 2020, 22, 169–183.

[44] TREMBECKA-WOJCIGA K., KOPERNIK M., SURMIAK M., MAJOR R., GAWLIKOWSKI M., BRUCKERT F., KOT M., LACKNER J.M., *Effect of the mechanical properties of carbon-based coatings on the mechanics of cell-material interactions*, Colloids Surf. B, 2021, 197, DOI: 10.1016/j.colsurfb.2020.111359.

[45] TYFA Z., JÓŹWIK P., OBIDOWSKI D., REOROWICZ P., JODKO D., KAPKA K., MAKOSIEJ R., CZKWIANIANC E., JÓŹWIK K., *Inhaled drug airflow patterns and particles deposition in the paediatric respiratory tract*, Acta Bioeng. Biomech., 2020, 22, 101–110.

[46] VAIDYA N., BARAGONA M., LAVEZZO V., MAESSEN R., VEROY K., *Simulation study of the cooling effect of blood vessels and*

blood coagulation in hepatic radiofrequency ablation, Int. J. Hyperther., 2021, 38, 95–104.

[47] VASAN S.S., GHOSH R., CUI Z., *Design of cone-and-plate test cell for ultrafiltration*, Desalination, 2002, 146, 219–224.

[48] YE C., ALI S., SUN Q., GUO M., LIU Y., GAO Y., HUO B., *Novel cone-and-plate flow chamber with controlled distribution of wall fluid shear stress*, Comput. Biol. Med., 2019, 106, 140–148.

[49] YU Z., TAN J., WANG S., *Enhanced discrete phase model for multiphase flow simulation of blood flow with high shear stress*, Sci. Prog., 2021, 104, DOI: 10.1177/00368504211008064.

[50] ZILLA P., DEUTSCH M., BEZUIDENHOUT D., DAVIES N.H., PENNEL T., *Progressive Reinvention or Destination Lost? Half a Century of Cardiovascular Tissue Engineering*, Front. Cardiovasc. Med., 2020, 7, DOI: 10.3389/fcvm.2020.00159.